White Matter Reference Region in PET Studies of ^{11}C-Pittsburgh Compound B Uptake: Effects of Age and Amyloid-β Deposition

Val J. Lowe[1], Emily S. Lundt[2], Matthew L. Senjem[1,3], Christopher G. Schwarz[1], Hoon-Ki Min[1], Scott A. Przybelski[2], Kejal Kantarci[1], David Knopman[4], Ronald C. Petersen[4], and Clifford R. Jack Jr.[1]

[1]Department of Radiology, Mayo Clinic, Rochester, Minnesota; [2]Division of Biostatistics, Department of Health Sciences Research, Mayo Clinic, Rochester, Minnesota; [3]Department of Information Technology, Mayo Clinic, Rochester, Minnesota; and [4]Department of Neurology, Mayo Clinic, Rochester, Minnesota

See an invited perspective on this article on page 1581.

Amyloid-β (Aβ) deposition as seen on PET using an Aβ-binding agent is a critical diagnostic biomarker for Alzheimer disease (AD). Some reports suggest using white matter (WM) as a reference region for quantification of serial Aβ PET studies; however, nonspecific WM retention in Aβ PET in people with dementia or cognitively unimpaired (CU) has been widely reported and is poorly understood. **Methods:** To investigate the suitability of WM as a reference region and the factors affecting WM ^{11}C-Pittsburgh compound B (^{11}C-PiB) uptake variability, we conducted a retrospective study on 2 large datasets: a longitudinal study of participants (n = 577) who were CU, had mild cognitive impairment, or had dementia likely due to AD; and a cross-sectional study of single-scan PET imaging in CU subjects (n = 1,349). In the longitudinal study, annual changes in WM ^{11}C-PiB uptake were assessed, and in the cross-sectional study, WM ^{11}C-PiB uptake was assessed relative to subject age. **Results:** Overall, we found that WM ^{11}C-PiB uptake showed age-related increases, which varied with the WM regions selected. Further, variable annual WM ^{11}C-PiB uptake changes were seen with different gray matter (GM) ^{11}C-PiB baseline uptake levels. **Conclusion:** WM binding increases with age and varies with GM ^{11}C-PiB. These correlations should be considered when using WM for normalization in ^{11}C-PiB PET studies. The cerebellar crus1+crus2 showed no increase with age and cerebellar GM+WM showed minimal increase, supporting their use as reference regions for cross-sectional studies comparing wide age spans. In longitudinal studies, the increase in WM uptake may be minimal in the short-term and thus using WM as a reference region in these studies seems reasonable. However, as participants age, the findings may be affected by changes in WM uptake. Changes in WM ^{11}C-PiB uptake may relate to disease progression, warranting examination of the causes of WM ^{11}C-PiB uptake.

Key Words: AD; ^{11}C-PiB; white matter; amyloid-β; PET

J Nucl Med 2018; 59:1583–1589
DOI: 10.2967/jnumed.117.204271

Amyloid-β (Aβ) plaque accumulation in the brain as measured by PET has become a critical diagnostic biomarker for Alzheimer disease (AD) (*1*). Given its implications for prognosis and potential early intervention (*2*), reliable quantitative measurement of Aβ deposition using PET has been an important topic of discussion (*3–5*).

For inter- and intrasubject semiquantitative Aβ PET imaging, obtaining the standardized uptake value ratio (SUVR) of cortical areas relative to a reference region was initially shown to closely mimic the Logan graphical distribution volume ratio shown in a ^{11}C-Pittsburgh compound B (^{11}C-PiB) Aβ PET study (*6*). For this reason, most large studies of Aβ deposition have used delayed imaging and have used the cerebellum as a reference region for normalization (*7*).

Recently, several longitudinal Aβ PET studies have suggested including white matter (WM) regions as reference areas for SUVR (*5,8–10*). Longitudinal ^{18}F-florbetapir Aβ PET studies report that as a reference region, WM has stronger correlations with cerebrospinal fluid $A\beta_{1–42}$ level and has less variability than the cerebellum (*8,10*). In addition, a cross-sectional ^{18}F-AV45 Aβ PET study showed that SUVR using the entire subcortical WM as a reference region had a higher correlation with distribution volume ratio than did SUVR of the cerebellum (*11*). In a ^{11}C-PiB PET study of AD patients at 3 different points in time, we showed that supratentorial WM with the cerebellum included was the most reliable reference region in representing disease progression over time (*5*).

The benefit of WM over the cerebellum as a reference region is that there is a larger region over which to average the signal, potentially leading to less noise. WM measurements may also be more resistant to small degrees of misregistration during image quantification (*12*). In addition, the cerebellar signal is collected at the edge of the scanner field of view where sensitivity is lower (*8,9*).

A pervasive finding in Aβ PET studies is the substantial retention of the tracer in the WM of both subjects with dementia and healthy controls (*13*). WM uptake has been observed with every Aβ PET imaging agent to a greater or lesser degree, independent of the presence of Aβ deposition (*14–17*). The mechanism of this binding is poorly understood, and its nonspecificity is attributed mainly to its nondisplaceable and nonsaturable characteristics seen in several ^{11}C-PiB PET studies (*7,18,19*).

Generally, WM uptake has not been a point of contention in disease categorization (*13*). However, because WM is being considered as a reference region, it is important to understand factors that affect WM uptake so as to assess its suitability for longitudinal studies for disease progression assessment and therapy evaluation studies in

Received Oct. 24, 2017; revision accepted Apr. 4, 2018.
For correspondence or reprints contact: Val J. Lowe, Department of Radiology, Mayo Clinic, Rochester, MN 55905.
E-mail: vlowe@mayo.edu
Published online Apr. 19, 2018.

TABLE 1
Participants Demographics

Variable	Longitudinal data			Cross-sectional data, CU
	CU	MCI	ADD	
No. of subjects	421	116	40	1,349
Mean age ± SD (y)	77 ± 7	75 ± 9	69 ± 11	71 ± 10
Age range (y)	51–94	54–90	50–91	50–95
Male (*n*)	256 (61%)	80 (69%)	24 (60%)	706 (52%)
Mean education ± SD (y)	15 ± 3	15 ± 4	15 ± 2	15 ± 3
Abnormal ^{11}C-PiB (*n*)	149 (35%)	73 (63%)	37 (92%)	429 (32%)
Mean global GM ^{11}C-PiB SUVR (crus, GM+WM, PVC) ± SD	1.5 ± 0.34	1.8 ± 0.53	2.2 ± 0.41	1.43 ± 0.31
APOE ε4 carrier (*n*)	115 (27%)	53 (46%)	24 (60%)	361 (27%)
Scans per person				
1				1,349 (100%)
2	300 (71%)	79 (68%)	26 (65%)	
3	101 (24%)	27 (23%)	7 (18%)	
4	17 (4%)	5 (4%)	5 (12%)	
5	3 (1%)	6 (5%)	2 (5%)	
Mean time between first and last scan ± SD (y)	2.8 ± 1.2	2.1 ± 1.1	1.9 ± 1.3	

crus = cerebellar crus1+crus2.

which changes in individual amyloid levels may be small and more easily affected by small changes in normalization region effects.

To investigate potential variables affecting WM ^{11}C-PiB uptake, we conducted a retrospective study evaluating the WM ^{11}C-PiB binding in 2 large population datasets: a longitudinal study of serial ^{11}C-PiB PET uptake in cognitively unimpaired (CU), mild cognitive impairment (MCI), and dementia likely due to AD (ADD) groups; and a cross-sectional study of single-scan ^{11}C-PiB imaging versus age in a CU group. Further, we evaluated annual WM ^{11}C-PiB uptake increases as they related to changes in gray matter (GM) uptake to assess its relationship to disease progression. These findings are discussed relative to the implications and potential confounds in using WM SUVR normalization and categorizing levels of amyloid deposition.

MATERIALS AND METHODS

Participants

Participants were drawn from the Mayo Clinic Study of Aging epidemiological study (*20*). The study was approved by Mayo Clinic and Olmstead Medical Center Institutional Review Boards, and all subjects signed an informed consent (Clinical trial #NCT00950430). Two large population datasets were extracted from this study: longitudinal data (n = 577); and cross-sectional data (n = 1,349) in which ^{11}C-PiB imaging was collected from 2006 to 2015, as described in Table 1. All subjects were categorized by neurologists, neuropsychologists, and study nurses through our consensus diagnosis using quantitative data from a brief mental status examination, 9 neuropsychological tests, and the Clinical Dementia Rating Scale (*20*). The longitudinal data consisted of subjects who were categorized as CU, MCI, or ADD. ADD is defined as being clinical diagnosis of Alzheimer disease without biomarker verification. Each clinical classification was further divided into Aβ-negative (A−) and Aβ-positive (A+) based on the global GM ^{11}C-PiB SUVR cutoff value of 1.4 SUVR (*21*). For the present analysis, we relabeled the study groups into A− (CU−, MCI−, and ADD−) and A+ (CU+, MCI+, and ADD+).

Imaging Method

^{11}C-PiB PET imaging was performed under Food and Drug Administration Investigational New Drug approval (#77924) and synthesized on-site at the Mayo Clinic Cyclotron Facility. ^{11}C-PiB PET/CT studies were performed as previously described in Lowe et al. (*22*), using GE scanners (Discovery 690XT and Discovery RX; GE Healthcare). Standard iterative reconstructions (256 matrix, 300 mm field of view, 1.17 × 1.17 × 3.27 mm voxel size) with corrections for attenuation, scatter, random coincidences, and radioactive decay were applied as well as a 5 mm Gaussian postfilter as previously described (*5*). T1-weighted MRI scans were acquired on 3-T scanners (Discovery MR750, Signa HDx, Signa HDxt, and Signa Excite; GE Healthcare) for region localization and masking, and for partial-volume correction (PVC).

Image and Statistical Analysis

MRI T1 and ^{11}C-PiB scans were coregistered using SPM12 with 6° of freedom. Resampling between MRI and PET resolutions was performed using ANTs software tools with third-order B-spline interpolation. Two-compartment PVC was applied for cerebrospinal fluid correction. Atlas regions of interest (ROIs) were resampled to subject spaces also using ANTs with nearest-neighbor interpolation (*5*).

ROI voxels that were deemed primarily nontissue according to the T1 MRI segmentations were omitted. Median values were computed for each of these regions and averaged, weighted by region size, to produce the composite median value. Two representative ROIs within WM were used for analysis as shown in Figure 1: periventricular and subcortical (*23*). These ROIs were subdivided to frontal, occipital, parietal, and temporal areas on the basis of the anatomic lobe discrimination of the STAND400 brain template (*24*). Additional ROIs were

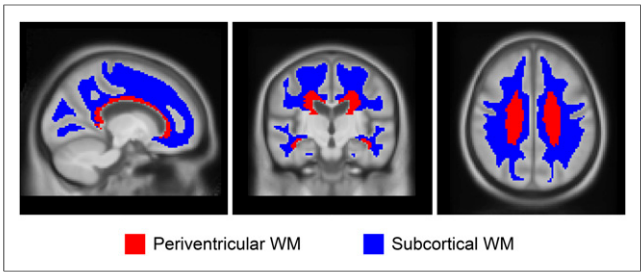

FIGURE 1. ROIs in WM. Two ROIs, periventricular and subcortical, within WM reference regions are shown.

used for comparison as well, including the corpus callosum (anterior and posterior), brain stem, cerebellum WM, and cerebellum WM+GM, as well as eroded subcortical WM and composite (voxel-weighted median average of cerebellum WM+GM, brain stem/pons, and eroded subcortical WM), which was designed to emulate regions from the paper by Landau et al. (*8*). The global GM ^{11}C-PiB ROI included GM of parietal, cingulate precuneus, prefrontal, orbitofrontal, temporal, and anterior cingulate regions (*25*). If not stated otherwise, the cerebellar crus1+crus2 voxel signal were used as the normalization region (denominator) for all SUVRs. In addition to and separate from the SUVR, we also assessed the SUV calculated from dose and weight normalization to describe the age associations of the ROIs. All analyses were conducted using R statistical software version 3.3.1 (*26*). Mixed-effects linear regression models using age at baseline as the time scale were used to estimate change in WM SUVR over time in the longitudinal dataset. Random subject-specific intercepts and slopes were included. We fit separate models for each region. To evaluate the effect of Aβ, a second linear mixed-effects model was fit including abnormal PiB and an abnormal PiB by time interaction. Together these fixed effects allowed WM SUVR to change with possibly different rates of decline by A− or A+ PiB status. All outcome measures were log-transformed to reduce skewness and to allow for interpretation of slope estimates as approximate annual percentage change (*27*). This procedure also enables the comparison of several different regions across a similar scale. We modeled the log of SUVR to estimate rate of accumulation expressed as percentage per year.

The age relationship to WM uptake was analyzed in a cross-sectional sample of CU subjects by fitting a linear regression model between age and SUV (or SUVR). To test for evidence of age-related differences between groups, we summarized the *P* values from an age by abnormal PiB interaction.

We compared annual change in global GM PiB SUVR and annual change in WM PiB SUVR using a 2-stage approach. First, we applied linear regression to examine the relationship between age and SUVR for each subject. The slope of the linear regression represents an estimate of the annual SUVR change for a given subject. Given the varying number of scans per subject, this technique has the advantage of allowing all scan data for a given subject to be used in the estimation of change. Change was estimated separately for global GM PiB SUVR and WM PiB SUVR, and the 2 measures were compared. To allow for differing rates of accumulation, we conducted linear regression between the 2 change measures by Aβ status, and the strength of association was determined by Pearson's correlation coefficient. Additionally, to compare annual WM PiB SUVR change and GM PiB SUVR at baseline, we calculated Spearman's correlations and fit local polynomial regression (loess) models to allow for nonlinear trends.

RESULTS

Annual WM ^{11}C-PiB SUVR Percentage Change in Longitudinal Data

The estimated annual WM ^{11}C-PiB SUVR percentage change using a linear mixed-effects model in the longitudinal data is shown in Figure 2 and Supplemental Table 1 (supplemental materials are available at http://jnm.snmjournals.org). Figure 2A shows annual WM ^{11}C-PiB SUVR percentage increase in CU, MCI, and ADD. The annual global GM ^{11}C-PiB SUVR showed a 1.9% increase. The subcortical WM area showed the highest annual percentage increase among the WM ROIs, ranging from 1.2% to 1.5%. The periventricular WM area showed annual increase ranging from 0.4% to 1.1%. The eroded subcortical WM and composite had a similar range as periventricular, having 0.9% and 0.6% annual increase, respectively. The corpus callosum (anterior and posterior), brain stem, and cerebellum WM annual increase ranged from 0.3% to 0.9%, with the cerebellum GM+WM showing the lowest annual increase of 0.2%. The slope is significantly different from 0 at the 0.05 level, if the 95% confidence interval excludes zero; therefore, all WM ROIs showed significant annual increases in SUVR percentage change.

Although both A− and A+ groups showed annual WM ^{11}C-PiB SUVR percentage increase, the increase rate varied between A− and A+ for each of the ROIs (Fig. 2B). The A+ group showed faster annual increase for the global GM (as would be expected from the cortical amyloid accumulation signal bleed-in) and subcortical WM (likely a bleed-in effect), whereas the A− group showed faster annual increase for the periventricular WM, corpus callosum, brain stem, cerebellum WM, and eroded subcortical WM. Cerebellum GM+WM showed no rate difference between A− and A+.

Age-Dependent WM Uptake Change in Cross-Sectional CU Data

To confirm whether the annual WM uptake increase is also observable in cross-sectional data, we selected a CU group

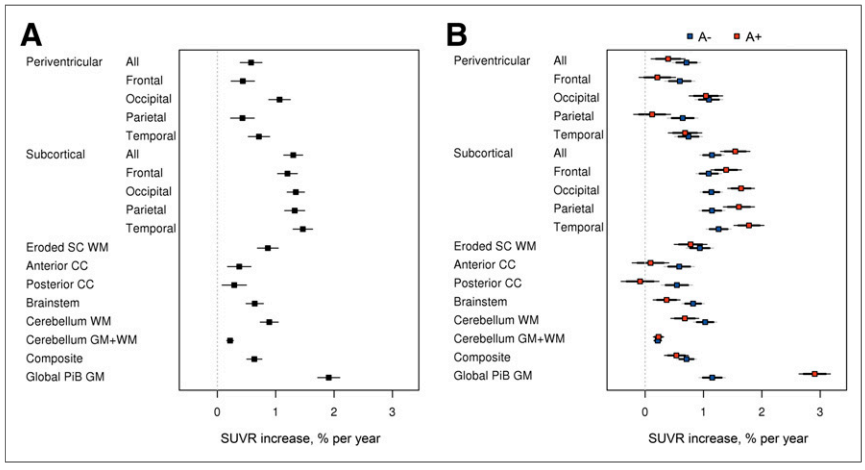

FIGURE 2. Annual WM ^{11}C-PiB SUVR percentage change in longitudinal data. (A) Regional increase in WM ^{11}C-PiB uptake. (B) Difference in WM accumulation (A− vs A+).

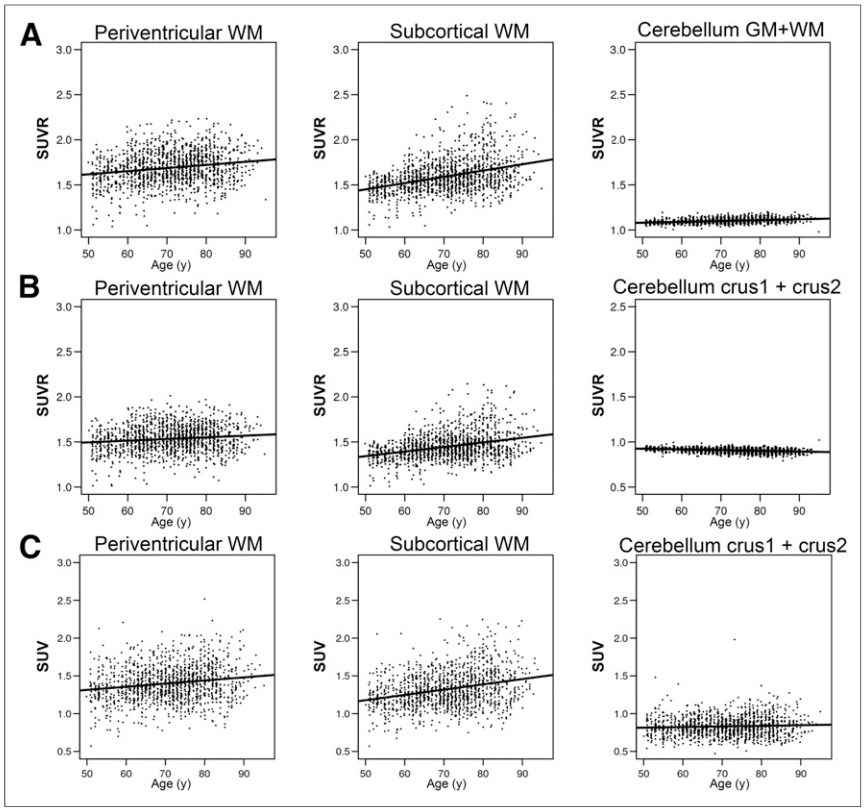

FIGURE 3. **Age**-dependent WM uptake change in cross-sectional CU data (SUVR and SUV). (A) Age and SUVR scatterplot with linear regression using cerebellum crus1+crus2 GM as reference region. (B) Age and SUVR scatterplot with linear regression using cerebellum GM+WM as reference region. (C) Age and SUV scatterplot with linear regression.

and compared the WM ^{11}C-PiB uptake related to age using different reference regions (Fig. 3; Supplemental Table 2). We confirmed an age-related increase in the periventricular WM SUVR (slope = 0.03, ρ = 0.19), subcortical WM SUVR (slope = 0.07, ρ = 0.37), and cerebellum GM+WM (slope = 0.01, ρ = 0.34) when normalized to cerebellar crus (Fig. 3A). Changing the reference region to cerebellum GM+WM showed a similar trend (Fig. 3B), with a trend toward a smaller slope in supratentorial WM, periventricular WM SUVR (slope = 0.02, ρ = 0.12), and subcortical WM SUVR (slope = 0.05, ρ = 0.33). The cerebellum crus1+crus2 GM slope (slope = −0.01, ρ = −0.31) became slightly negative with the inclusion of the cerebellar WM in the denominator. In addition to and separate from the SUVR, we assessed SUV with age as an alternate normalization method. The SUV of periventricular (slope = 0.04, ρ = 0.17), subcortical (slope = 0.07, ρ = 0.28), and cerebellum crus1+crus2 (slope = 0.01, ρ = 0.06) regions showed slopes similar to those of SUVR normalization (Fig. 3C; Supplemental Table 2). Finally, we evaluated the cerebellar reference region atrophy effect by applying 3-compartment PVC to the cerebellar GM reference region (atrophy corrected) and confirmed the WM age trend was still present and that the slope was similar to that of the 2-compartment PVC results (atrophy uncorrected) (Supplemental Fig. 1).

Comparing Annual WM ^{11}C-PiB SUVR Change with Annual GM ^{11}C-PiB SUVR Change

We saw a correlation between annual WM ^{11}C-PiB SUVR change and annual global GM ^{11}C-PiB SUVR change in the longitudinal data shown in Figure 4. Periventricular WM showed a correlation between annual WM and global GM ^{11}C-PiB SUVR change (A−: slope = 1.21, $P <$ 0.001 and A+: slope = 0.69, $P <$ 0.001). Subcortical WM showed correlation between annual WM and global GM ^{11}C-PiB SUVR change (A−: slope = 1.07, $P <$ 0.001 and A+: slope = 0.76, $P <$ 0.001). Cerebellum GM+WM showed low correlation with the global GM ^{11}C-PiB SUVR change (A−: slope = 0.16, $P <$ 0.001 and A+: slope = 0.08, $P <$ 0.001).

Comparing Annual WM ^{11}C-PiB SUVR Change with GM ^{11}C-PiB SUVR Baseline Values

Figure 5 shows the relationship between the annual WM uptake change and baseline GM ^{11}C-PiB in the longitudinal data. Depending on the global GM ^{11}C-PiB SUVR baseline, there are different rates in the annual WM ^{11}C-PiB SUVR change. In A+ participants, both ROIs (periventricular WM and subcortical WM) showed a trend of greatest change in the WM ^{11}C-PiB annual increase at 1.9–2.1 GM ^{11}C-PiB SUVR baseline values, and the rate showed decrease at the higher GM ^{11}C-PiB SUVR baseline levels (>∼2.7). At the lowest global GM ^{11}C-PiB SUVR baseline values (representing the A− group [blue circles]), increases of WM ^{11}C-PiB annual change for both periventricular and subcortical WM ROIs were the highest. The relationship between within-subject annual

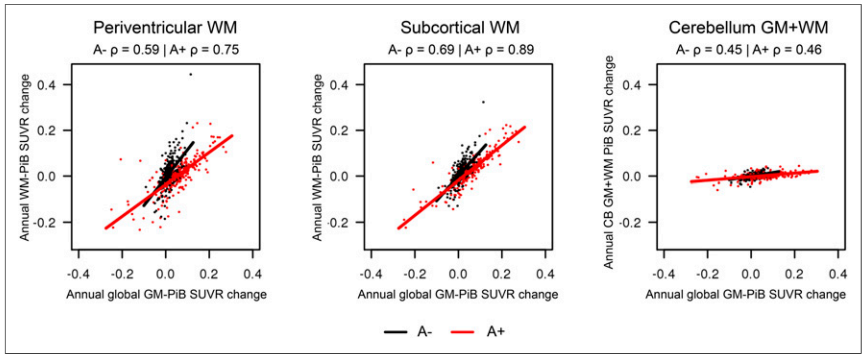

FIGURE 4. Comparison of annual WM ^{11}C-PiB SUVR change with annual GM ^{11}C-PiB SUVR change. Scatterplot between annual change in global GM ^{11}C-PiB SUVR and annual change in regional WM ^{11}C-PiB SUVR by Aβ status with linear regression line among A− (black) and A+ (red).

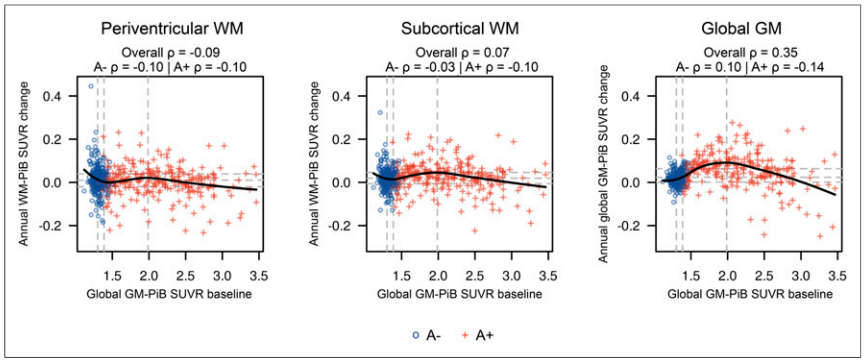

FIGURE 5. Comparison of annual WM uptake change and baseline global GM ^{11}C-PiB in longitudinal data. Spearman correlations of Loess curve are shown at top of each panel over all subjects, among A− (blue) and A+ (red).

SUVR change and baseline age had no distanced effect, implying the annual increase rate itself shows minimum age related effect (Supplemental Fig. 2).

DISCUSSION

The causes of WM ^{11}C-PiB uptake in Aβ PET imaging remain largely unknown, but its effects are important to understand when WM is used as a normalization region for quantification of cortical Aβ tracer binding. Changes over time in WM uptake could affect cortical GM SUVR results. In this study, we found that WM ^{11}C-PiB uptake increases with age and varies with GM Aβ deposition and with the area of WM sampled.

The simplest explanation for some variations in signal in subcortical WM ^{11}C-PiB would be spillover of the GM Aβ signal into subcortical WM because this region includes the area of WM closest to GM. The fact that the subcortical WM had the highest annual increase and a steeper age-dependent increase compared with periventricular WM would support this, as would the fact that the A+ group had a greater annual uptake increase in subcortical WM than the A− group. For this reason, investigators using WM as a reference region tend to avoid selecting WM regions close to GM (*5,8,9*). Our results support this approach in that we observed a lower level of annual ^{11}C-PiB uptake increase in periventricular or eroded subcortical WM ROIs in both longitudinal and cross-sectional samples.

Nevertheless, annual WM ^{11}C-PiB increases are seen in periventricular WM and other WM regions such as corpus callosum, cerebellum WM, and also in eroded subcortical WM. These values are moderate (0.4%–1.1%) compared with the annual GM increase (1.9%), but are statistically significant. These increases are found in both A− and A+ populations and appear in WM areas at a great enough distance from GM that cannot be explained by a GM spillover effect.

The relatively slower kinetics of WM than GM, which results in a slower clearance rate (*13,18*), may explain WM ^{11}C-PiB uptake. This could also explain the age-related increase in WM ^{11}C-PiB binding, because cerebral perfusion on average declines with age (*28*), thus slowing WM clearance of the tracer in old versus young. Blood flow has been reported to be slower in WM than GM (*29,30*). Delays in delivery (*31*) and slower clearance of the tracers (*32*) in WM have been previously described in molecular imaging studies. For example, ^{11}C-PiB clearance was reported to be slower in WM than GM in AD and CU subjects (*18*).

Studies using MRI to measure white matter hyperintensity have proposed that cerebral small-vessel disease can lead to reduced Aβ clearance and to increased cerebral GM ^{11}C-PiB in AD (*33,34*). However, white matter hyperintensity measurements in studies of WM ^{11}C-PiB uptake have found reduction in binding (*35*) and that WM lesions can reduce WM ^{11}C-PiB binding in cognitively impaired (*36*) as well as in multiple sclerosis patients (*37*).

Another possible explanation of WM uptake may be the lipophilic nature of Aβ PET tracers that may enhance binding of the high lipid content of WM (*7*). This possibility is further supported by histopathologic studies (*38*). However, given the generally agreed on concept of age-related myelin loss, our age-related WM ^{11}C-PiB uptake increase is not explained by this theory. These data are inconsistent with our findings, and our work suggests that alternate mechanisms must be at play to explain the increased uptake of WM ^{11}C-PiB with age.

One of the findings in our study was that the annual increase in WM ^{11}C-PiB uptake correlated with annual increases in GM ^{11}C-PiB uptake in WM regions even when spillover is an unlikely component (periventricular WM). The trends in GM change with age were previously reported in a comparison of annual increase in GM ^{11}C-PiB uptake with GM baseline SUVR (*21*) but have not been described previously for WM annual change.

Previously, ^{11}C-PiB was also shown to bind a wide range of fibrillar Aβ pathology, including diffuse plaques and cerebrovascular amyloid angiopathy, which affects both GM and WM (*39*). Diffuse plaques are common in the brains of elderly individuals and can be seen in relatively large numbers in the absence of any associated evidence of cognitive impairment and could be a WM component to ^{11}C-PiB binding in some (*40–42*).

We used 2-compartmental PVC correction in this study, correcting only for cerebrospinal fluid (*43*). It would be possible to use more sophisticated PVC methods, such as geometric transfer matrix (*44*), in an attempt to measure the WM signal, but geometric transfer matrix PVC assumes that individual regions each have homogeneous uptake, which is a questionable assumption for PiB in WM. Instead, in our analysis, we opted to include eroded subcortical WM ROI and other variants, which consist of voxels that were sufficiently far from the cortex so as to ensure that bleed-in of the cortical signal was not a factor in the measured signal.

The implications of the present findings are that the use of WM normalization could affect the characterization of A+ or A− subjects and the quantification of Aβ accumulation over time. The cerebellar crus1+crus2 showed no increase with age, and cerebellar GM+WM showed minimal increase, supporting their use as reference regions for cross-sectional studies comparing wide age spans. Relative to longitudinal studies, the increase in WM uptake over the short-term may be minimal, but as the longitudinal observation continues for a longer time frame, the results may be affected by changes in WM uptake. For example, the WM annual increase maximized within A+ individuals at a GM baseline SUVR range of 1.9–2.1. The highest WM increase in the

entire population was seen when global GM ^{11}C-PiB SUVRs were the lowest in A− individuals. In contrast, individuals with higher GM ^{11}C-PiB SUVR baseline levels (~2.7 >) showed a trend of annual WM decrease. These data demonstrate that the annual WM change rate varies based on population selection with different amyloid status and different age ranges.

These observations may also help to reconcile findings related to seeing better stabilities in longitudinal Aβ PET studies when using WM normalization (*5,8,9*), where the reports describe 5 y or less of serial PET images. In a short-term longitudinal study (<5 y), the improved noise characteristics of a large WM normalization region would add stability and hence reliability, therefore may be beneficial (i.e., a small WM rate change in those with a GM SUVR range of 2.1–2.7 would add to stability). It could also be the case that small GM Aβ accumulation could be masked by WM increase, leading to the impression of improved reliability, especially when reliability is compared against cognitive change (i.e., participants with no or minimal cognitive change could still have Aβ accumulation).

For longer term longitudinal study, age-related increases in WM will ultimately result in underestimation of longitudinal GM increases in most populations (i.e., overly conservative estimation). Possible approaches suggested by these data for longitudinal data include using deep WM for short-term datasets or age correction in the WM region. More longitudinal data and additional analyses would be needed to test the utility of age correction for reference regions.

CONCLUSION

We found that WM ^{11}C-PiB uptake has notable variability among those who are cognitively unimpaired (with and without evidence of Aβ deposition) and those diagnosed with either MCI or ADD. WM ^{11}C-PiB uptake increases with age and is seen in both cross-sectional and serial evaluations. These findings are important relative to the quantitative and visual interpretation of ^{11}C-PiB PET scans. The variability of WM ^{11}C-PiB uptake may hamper accurate characterization. Increases in WM ^{11}C-PiB uptake over time appear to occur in association with increasing global GM ^{11}C-PiB SUVR, even in WM ROIs far from GM. Eroded subcortical WM and composite regions (cerebellum WM+GM, brain stem/pons, and eroded subcortical WM) are an important consideration to reduce but not eliminate WM ^{11}C-PiB uptake effects. This study was specific to Aβ PET imaging using ^{11}C-PiB, and thus future investigations should address the characteristics of other Aβ tracers.

DISCLOSURE

This work was supported by NIH grants P50 AG16574, U01 AG06786, R01 AG11378, and R01 AG041851; the Elsie and Marvin Dekelboum Family Foundation; GHR Foundation; and the Robert H. and Clarice Smith and Abigail Van Buren Alzheimer's Disease Research Program of the Mayo Foundation. Dr. Lowe is a consultant for Bayer Schering Pharma and Piramal Imaging Inc. and receives research support from GE Healthcare, Siemens Molecular Imaging, and AVID Radiopharmaceuticals. Dr. Knopman serves on a Data Safety Monitoring Board for the DIAN study and is an investigator in clinical trials sponsored by Biogen, Lilly Pharmaceuticals, and the Alzheimer's Disease Cooperative Study. Dr. Petersen serves on scientific advisory boards for Pfizer, Inc., Janssen Alzheimer Immunotherapy, Elan Pharmaceuticals, and GE Healthcare. No other potential conflict of interest relevant to this article was reported.

ACKNOWLEDGMENTS

We thank David Jones, MD, and Bradley Boeve, MD, for their valuable comments and suggestions. We thank Penelope Duffy, PhD, for her editorial contributions. We thank Ping Fang, PhD, for synthesizing ^{11}C-PiB.

REFERENCES

1. McKhann GM, Knopman DS, Chertkow H, et al. The diagnosis of dementia due to Alzheimer's disease: recommendations from the National Institute on Aging-Alzheimer's Association workgroups on diagnostic guidelines for Alzheimer's disease. *Alzheimers Dement.* 2011;7:263–269.
2. Jack CR Jr, Knopman DS, Jagust WJ, et al. Tracking pathophysiological processes in Alzheimer's disease: an updated hypothetical model of dynamic biomarkers. *Lancet Neurol.* 2013;12:207–216.
3. Klunk WE, Koeppe RA, Price JC, et al. The Centiloid Project: standardizing quantitative amyloid plaque estimation by PET. *Alzheimers Dement.* 2015;11:1-15 e11-14.
4. Schmidt ME, Chiao P, Klein G, et al. The influence of biological and technical factors on quantitative analysis of amyloid PET: points to consider and recommendations for controlling variability in longitudinal data. *Alzheimers Dement.* 2015;11:1050–1068.
5. Schwarz CG, Senjem ML, Gunter JL, et al. Optimizing PiB-PET SUVR change-over-time measurement by a large-scale analysis of longitudinal reliability, plausibility, separability, and correlation with MMSE. *Neuroimage.* 2017;144:113–127.
6. McNamee RL, Yee SH, Price JC, et al. Consideration of optimal time window for Pittsburgh compound B PET summed uptake measurements. *J Nucl Med.* 2009;50:348–355.
7. Klunk WE, Engler H, Nordberg A, et al. Imaging brain amyloid in Alzheimer's disease with Pittsburgh compound-B. *Ann Neurol.* 2004;55:306–319.
8. Landau SM, Fero A, Baker SL, et al. Measurement of longitudinal β-amyloid change with ^{18}F-florbetapir PET and standardized uptake value ratios. *J Nucl Med.* 2015;56:567–574.
9. Chen K, Roontiva A, Thiyyagura P, et al. Improved power for characterizing longitudinal amyloid-β PET changes and evaluating amyloid-modifying treatments with a cerebral white matter reference region. *J Nucl Med.* 2015;56:560–566.
10. Shokouhi S, McKay JW, Baker SL, et al. Reference tissue normalization in longitudinal ^{18}F-florbetapir positron emission tomography of late mild cognitive impairment. *Alzheimers Res Ther.* 2016;8:2.
11. Ottoy J, Verhaeghe J, Niemantsverdriet E, et al. Validation of the semi-quantitative static SUVR method for [^{18}F]-AV45 PET by pharmacokinetic modeling with an arterial input function. *J Nucl Med.* 2017;58:1483–1489.
12. Schwarz CG, Jones DT, Gunter JL, et al. Contributions of imprecision in PET-MRI rigid registration to imprecision in amyloid PET SUVR measurements. *Hum Brain Mapp.* April 22, 2017 [Epub ahead of print].
13. Kepe V, Moghbel MC, Langstrom B, et al. Amyloid-beta positron emission tomography imaging probes: a critical review. *J Alzheimers Dis.* 2013;36:613–631.
14. Forsberg A, Engler H, Almkvist O, et al. PET imaging of amyloid deposition in patients with mild cognitive impairment. *Neurobiol Aging.* 2008;29:1456–1465.
15. Vandenberghe R, Van Laere K, Ivanoiu A, et al. ^{18}F-flutemetamol amyloid imaging in Alzheimer disease and mild cognitive impairment: a phase 2 trial. *Ann Neurol.* 2010;68:319–329.
16. Wong DF, Rosenberg PB, Zhou Y, et al. In vivo imaging of amyloid deposition in Alzheimer disease using the radioligand ^{18}F-AV-45 (florbetapir [corrected] F 18). *J Nucl Med.* 2010;51:913–920.
17. Villemagne VL, Mulligan RS, Pejoska S, et al. Comparison of ^{11}C-PiB and ^{18}F-florbetaben for Abeta imaging in ageing and Alzheimer's disease. *Eur J Nucl Med Mol Imaging.* 2012;39:983–989.
18. Fodero-Tavoletti MT, Rowe CC, McLean CA, et al. Characterization of PiB binding to white matter in Alzheimer disease and other dementias. *J Nucl Med.* 2009;50:198–204.
19. Catafau AM, Bullich S. Amyloid PET imaging: applications beyond Alzheimer's disease. *Clin Transl Imaging.* 2015;3:39–55.
20. Roberts RO, Geda YE, Knopman DS, et al. The Mayo Clinic Study of Aging: design and sampling, participation, baseline measures and sample characteristics. *Neuroepidemiology.* 2008;30:58–69.

21. Jack CR Jr, Wiste HJ, Weigand SD, et al. Defining imaging biomarker cut points for brain aging and Alzheimer's disease. *Alzheimers Dement.* 2017;13: 205–216.
22. Lowe VJ, Kemp BJ, Jack CR Jr, et al. Comparison of ^{18}F-FDG and PiB PET in cognitive impairment. *J Nucl Med.* 2009;50:878–886.
23. Murray ME, Senjem ML, Petersen RC, et al. Functional impact of white matter hyperintensities in cognitively normal elderly subjects. *Arch Neurol.* 2010;67: 1379–1385.
24. Vemuri P, Gunter JL, Senjem ML, et al. Alzheimer's disease diagnosis in individual subjects using structural MR images: validation studies. *Neuroimage.* 2008;39:1186–1197.
25. Jack CR Jr, Wiste HJ, Lesnick TG, et al. Brain beta-amyloid load approaches a plateau. *Neurology.* 2013;80:890–896.
26. Team RC. R: A Language and Environment for Statistical Computing. 2013. The R Foundation website. https://www.r-project.org/about.html. Accessed August 17, 2018.
27. Gelman A, Hill J. *Data Analysis Using Regression and Multilevel/Hierarchical Models.* New York, NY: Cambridge University Press; 2007.
28. Fisher JP, Hartwich D, Seifert T, et al. Cerebral perfusion, oxygenation and metabolism during exercise in young and elderly individuals. *J Physiol (Lond).* 2013;591:1859–1870.
29. van Gelderen P, de Zwart JA, Duyn JH. Pittfalls of MRI measurement of white matter perfusion based on arterial spin labeling. *Magn Reson Med.* 2008;59:788–795.
30. Liu P, Uh J, Devous MD, Adinoff B, Lu H. Comparison of relative cerebral blood flow maps using pseudo-continuous arterial spin labeling and single photon emission computed tomography. *NMR Biomed.* 2012;25:779–786.
31. Ibaraki M, Shimosegawa E, Toyoshima H, et al. Effect of regional tracer delay on CBF in healthy subjects measured with dynamic susceptibility contrast-enhanced MRI: comparison with ^{15}O-PET. *Magn Reson Med Sci.* 2005;4:27–34.
32. Ichise M, Golan H, Ballinger JR, Vines D, Blackman A, Moldofsky H. Regional differences in technetium-99m-ECD clearance on brain SPECT in healthy subjects. *J Nucl Med.* 1997;38:1253–1260.
33. Grimmer T, Faust M, Auer F, et al. White matter hyperintensities predict amyloid increase in Alzheimer's disease. *Neurobiol Aging.* 2012;33:2766–2773.
34. Prins ND, Scheltens P. White matter hyperintensities, cognitive impairment and dementia: an update. *Nat Rev Neurol.* 2015;11:157–165.
35. Goodheart AE, Tamburo E, Minhas D, et al. Reduced binding of Pittsburgh Compound-B in areas of white matter hyperintensities. *Neuroimage Clin.* 2015; 9:479–483.
36. Glodzik L, Rusinek H, Li J, et al. Reduced retention of Pittsburgh compound B in white matter lesions. *Eur J Nucl Med Mol Imaging.* 2015;42:97–102.
37. Zeydan B, Lowe VJ, Schwarz CG, et al. Pittsburgh compound-B PET white matter imaging and cognitive function in late multiple sclerosis. *Mult Scler.* 2018; 24:739–749.
38. Stankoff B, Freeman L, Aigrot MS, et al. Imaging central nervous system myelin by positron emission tomography in multiple sclerosis using [methyl-^{11}C]-2-(4′-methylaminophenyl)- 6-hydroxybenzothiazole. *Ann Neurol.* 2011;69:673–680.
39. Lockhart A, Lamb JR, Osredkar T, et al. PIB is a non-specific imaging marker of amyloid-beta (Abeta) peptide-related cerebral amyloidosis. *Brain.* 2007;130: 2607–2615.
40. Gentleman SM, Bruton C, Allsop D, Lewis SJ, Polak JM, Roberts GW. A demonstration of the advantages of immunostaining in the quantification of amyloid plaque deposits. *Histochemistry.* 1989;92:355–358.
41. Wolf DS, Gearing M, Snowdon DA, Mori H, Markesbery WR, Mirra SS. Progression of regional neuropathology in Alzheimer disease and normal elderly: findings from the Nun study. *Alzheimer Dis Assoc Disord.* 1999;13:226–231.
42. Morris JC, Storandt M, McKeel DW Jr, et al. Cerebral amyloid deposition and diffuse plaques in "normal" aging: Evidence for presymptomatic and very mild Alzheimer's disease. *Neurology.* 1996;46:707–719.
43. Meltzer CC, Leal JP, Mayberg HS, Wagner HN Jr, Frost JJ. Correction of PET data for partial volume effects in human cerebral cortex by MR imaging. *J Comput Assist Tomogr.* 1990;14:561–570.
44. Sattarivand M, Kusano M, Poon I, Caldwell C. Symmetric geometric transfer matrix partial volume correction for PET imaging: principle, validation and robustness. *Phys Med Biol.* 2012;57:7101–7116.